MODULE VI: A Rate-Adaptive (VVIR) Cardiac Pacemaker with Accelerometer-Based Activity Sensing

Lance Lindsey, Ege Ozemek
Group 10
BME 354L - April 21, 2026

INTRODUCTION

Background

The cardiac conduction system propagates depolarization from the sinoatrial (SA) node through the atria, the atrioventricular (AV) node, and then through the His–Purkinje system to excite the ventricles in a coordinated sequence [1]. Disruptions to this system can produce bradyarrhythmias in which the ventricular rate is too slow to meet metabolic demand. Complete (third-degree) atrioventricular block, for instance, fully severs conduction between the atria and ventricles, leaving the ventricles to depolarize at an intrinsic escape rate of 20-40 bpm [2]. SA node dysfunction and symptomatic sinus bradycardia produce similar hemodynamic consequences. In each case, the heart cannot respond to increased metabolic demand, and untreated patients experience syncope, fatigue, or sudden cardiac death.

An artificial cardiac pacemaker addresses these arrhythmias by sensing intrinsic electrical activity and delivering a suprathreshold electrical stimulus to the myocardium when the intrinsic rate falls below a clinician-programmed lower rate limit [3]. Modern pacemakers are classified by the NASPE/BPEG generic code, which encodes the paced chamber, sensed chamber, response to sensing, and rate modulation in a four-letter designation [4]. A key clinical limitation of fixed-rate pacing (VVI) is that it cannot accommodate chronotropic demand during exercise, and rate-adaptive pacing (VVIR) addresses this limitation by using a physiological sensor, most commonly an accelerometer, to modulate the pacing rate in response to patient activity [5].

Approach

This report describes the design, characterization, and in vivo demonstration of a VVIR cardiac pacemaker implemented on an Arduino Nano Every microcontroller with discrete analog sensing and stimulation front ends. The system measures the frog cardiac electrogram via a three-stage instrumentation-filter–amplifier chain, detects each ventricular depolarization with a comparator-based R-wave detector, and executes VVI pacing logic at a firmware-controlled lower rate interval (LRI). When no intrinsic beat is detected within the LRI, the microcontroller triggers a MOSFET-switched capacitive-discharge stimulator to deliver a rectangular current pulse of duration equal to twice the measured chronaxie, as determined in Module III. The added VVIR functionality is implemented with an ADXL335 three-axis accelerometer whose vector-magnitude output continuously updates the LRI between a resting rate of 60 bpm and a peak-activity rate of 120 bpm. System performance was characterized stage by stage on the bench and demonstrated end-to-end in vivo on a pithed frog preparation, with the device successfully pacing the myocardium when the intrinsic rate fell below the programmed LRI.

PACEMAKER DESIGN

Sensing Circuitry

The cardiac electrogram is measured differentially with two Ag/AgCl electrodes placed on the frog myocardium and amplified by an AD620 instrumentation amplifier configured for a nominal gain of 10 V/V. The instrumentation amplifier's high input impedance and common-mode rejection prevent electrode loading and reject 60 Hz line interference picked up by the long electrode leads. The output of the instrumentation amplifier feeds a passive first-order high-pass filter (R_HPF = 150 kΩ, C = 1 μF, f_c = 1.06 Hz) that removes DC offsets and baseline drift caused by electrode half-cell potentials, followed by a passive first-order low-pass filter (R_LPF = 3.3 kΩ, C = 1 μF, f_c = 48.2 Hz) that attenuates high-frequency electrode motion artifact and residual 60 Hz interference. A second non-inverting amplifier stage based on an LM358 op-amp provides an additional gain of approximately 100 V/V, bringing the total midband gain of the sensing chain to roughly 1000 V/V so that the millivolt-scale frog electrogram spans a usable fraction of the 0-5 V microcontroller ADC range. The final stage is an LM358 comparator referenced against a threshold set by a voltage divider from the 5 V rail; its open-drain output swings rail-to-rail and produces a clean digital pulse on each detected depolarization.

The sensing chain was characterized by stage rather than end-to-end because the high overall gain would saturate the oscilloscope input for any single-frequency test signal large enough to be resolved across all stages. The instrumentation amplifier gain was verified by applying a 10 mV, 10 Hz sinusoid from the function generator and measuring the output as a 100 mV peak-to-peak waveform. Filter cutoffs were characterized by sweeping a 100 mV sinusoid from 0.1 Hz to 200 Hz and recording the -3 dB points. The comparator was verified independently with a manually applied threshold crossing, confirming rail-to-rail switching. The predicted end-to-end response, computed from the cascaded stage transfer functions, is shown in Figure 1.

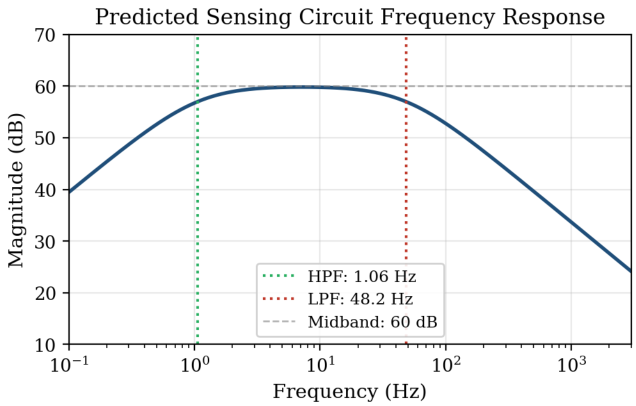

Figure 1. Predicted frequency response of the full sensing chain (cascaded analytical model). The midband gain is approximately 60 dB, with the -3 dB corners at 1.06 Hz and 48.2 Hz spanning the physiological bandwidth of the frog electrogram.

Acquisition and Processing

The amplified electrogram is sampled on the Arduino's analog input A0 at a software-controlled rate of 200 Hz, which provides at least ten samples across the sharp depolarization spike of the frog electrogram and satisfies the Nyquist criterion for the 50 Hz low-pass cutoff of the sensing chain. The comparator output is wired to digital input D2, where a rising-edge external interrupt latches a millisecond-resolution timestamp for each detected R-wave. A refractory period of 100 ms is enforced in the interrupt service routine to reject the decaying tail of each electrogram and the large post-stimulus recovery transient that would otherwise retrigger the comparator; this value was experimentally optimized during the April 17 bench demonstration, where shorter refractory periods produced erroneous double-counting (manifesting as aliased R-R intervals near 250-300 ms) and longer periods missed legitimate beats at elevated heart rates. The R-R interval is computed from the difference between consecutive timestamps and, together with the instantaneous heart rate, streamed to the host computer over USB-serial at 9600 baud for display on an OLED and for later offline analysis.

VVI Pacing Logic

The firmware maintains a rolling LRI timer that is reset on every event, either a sensed natural beat or a delivered pace. If the timer reaches the current LRI without an intervening sense event, the microcontroller drives digital output D4 high for a fixed pulse duration, then returns low. The VVI logic thus paces when the intrinsic rhythm is inadequate and inhibits pacing when the intrinsic rate exceeds the programmed lower rate, the main behavior of the NASPE VVI mode.

The firmware pulse width was set to 150 ms, which is substantially longer than the 2c = 21 ms suggested by the Module III chronaxie fit (c = 10.3 ms). The decision to use 150 ms rather than 21 ms was made on the bench during initial integration testing. With the shorter 21 ms pulse, we observed intermittent capture failures in the in vivo preparation, likely because the actual capture threshold at the tissue-electrode interface is higher than the bench strength-duration curve would predict once electrode polarization, electrode geometry, and in vivo loading are considered. Commercial pacemakers routinely program pulse widths of 0.4-1.0 ms because they deliver tens of milliamps through optimized endocardial leads with very low interface impedance; our discrete surface-electrode setup delivers only ~1.4 mA peak current, so increasing pulse duration is the direct lever we have for ensuring reliable capture. At 150 ms pulse width and 1.4 mA delivered current, the per-pulse charge is approximately 210 nC - well above the 2b·2c charge-minimum of ~1.9 nC from the Module III fit - and this margin proved necessary for reliable capture in the April 17 demonstration.

Stimulation Circuitry

The digital pacing output drives the gate of a 2N7000 n-channel enhancement-mode MOSFET through a 100 Ω gate resistor, which damps parasitic oscillations during the switching edge without limiting DC drive (the MOSFET gate is capacitive rather than current-driven). The MOSFET acts as a low-side switch that connects a 10 µF capacitor, trickle-charged through a 75 kΩ series resistor from the 9 V supply, to the tissue load. When the gate is pulsed high, the capacitor discharges through the myocardium as a rectangular current pulse whose duration is set by the Arduino pulse width and whose amplitude is set by the charged capacitor voltage and tissue impedance. The 10 µF value was selected in Module V.2 because the corresponding discharge time constant ($\tau = R\_L \cdot C = 0.75$ s) is far longer than the 150 ms pulse width, so the capacitor voltage sags by less than 5% during any single stimulus and the waveform approximates an ideal rectangular pulse. Between pulses the capacitor recharges through the 75 kΩ resistor; at the highest pacing rate of 300 bpm the inter-pulse interval of 200 ms is much shorter than the recharge time constant, but Module V.2 measurements confirmed that sufficient charge replenishes between pulses to maintain the delivered peak voltage within 1% across the 60-300 bpm range.

Added Functionality: VVIR Rate Adaptation

Rate-adaptive (VVIR) pacing augments the fixed-rate VVI algorithm with a physiological sensor that modulates the LRI in real time to match metabolic demand. Commercial pacemakers from Medtronic, Boston Scientific, and Abbott use piezoelectric or MEMS accelerometers for this purpose [5], and this implementation follows the same architecture. An ADXL335 three-axis analog accelerometer is mounted on the device enclosure with its X, Y, and Z outputs wired to Arduino analog inputs A1-A3. Every loop iteration, the firmware reads the three axes, subtracts the 1.65 V DC offset corresponding to 0 g, computes the vector magnitude $\sqrt{(X^2 + Y^2 + Z^2)}$ of the AC component, and maps the result onto a target rate between 60 and 120 bpm via a linear transform between calibrated ACTIVITY_MIN and ACTIVITY_MAX bounds. The new LRI (60000 / target_rate) is then applied to the next timing cycle. Because the rate adaptation runs in parallel with the core VVI logic rather than replacing it, sensed beats still inhibit paced output in the normal manner. The full firmware listing is provided in Appendix A.

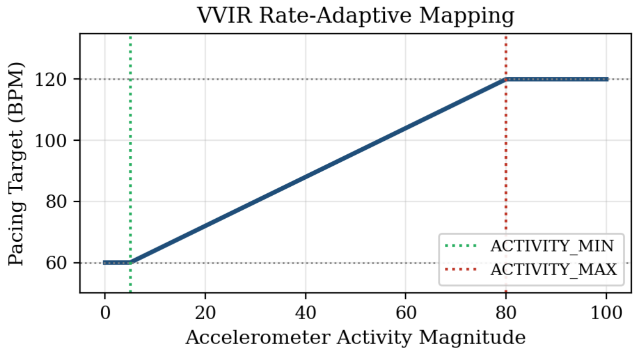

Figure 2. VVIR activity-to-rate mapping. Accelerometer vector magnitude is clipped to the calibrated window [ACTIVITY_MIN, ACTIVITY_MAX] and linearly mapped to a pacing target between 60 bpm (rest) and 120 bpm (peak activity).

System Integration and Testing

End-to-end testing proceeded in three stages. First, each analog and digital block was characterized individually on the bench against a benchtop ECG simulator (Fluke MPS450) to verify gain, cutoff, detection latency, and pulse fidelity. Second, the integrated system was dry-run with the simulator sourcing synthetic ECG at 60, 90, 120, 150, 170, and 180 bpm into the sensing input while the stimulator output was captured on an oscilloscope, verifying that the measured R-R intervals matched the programmed LRIs and that the VVI inhibition behavior correctly suppressed pacing when intrinsic rate exceeded target. Third, the system was connected to a double-pithed frog preparation on April 17, 2026, with sensing and stimulation electrodes applied directly to the ventricle, and the full VVIR algorithm was exercised end-to-end.

TESTING AND RESULTS

Sensing: Electrogram Measurement

Figure 3 shows a representative 14 s segment of the amplified frog cardiac electrogram recorded during the April 17 in vivo demonstration. The trace exhibits the characteristic biphasic morphology of the frog ventricular depolarization, a sharp positive spike followed by a narrower negative deflection, with a peak-to-peak amplitude of approximately 2.5 V at the output of the sensing chain, corresponding to an electrode-level signal of roughly 2.5 mV given the circuit's midband gain. The intrinsic cycle length averages approximately 1.2 s (50 bpm), which is within the expected range for a pithed frog at room temperature.

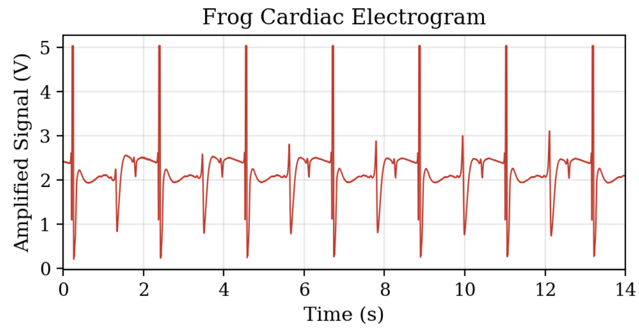

Figure 3. Amplified frog cardiac electrogram recorded during the April 17 in vivo demonstration. Periodic sharp depolarizations are clearly resolved above the quiescent baseline, with no visible 60 Hz interference.

Acquisition: R-R Detection Accuracy

The real-time R-R detection accuracy was characterized against the Fluke MPS450 ECG simulator at six programmed rates spanning 60-180 bpm. For each setting, at least 30 consecutive R-R intervals were captured from the serial output and the median was compared with the expected interval (60000 / BPM). Results are summarized in Table 1 and plotted in Figure 4. The measured R-R intervals track the expected values with better than 1% error across the full tested range, confirming that the interrupt-driven detection is accurate and that the 200 Hz sampling rate faithfully captures the electrogram at physiologically relevant heart rates. The small negative bias (~ 0.3-0.7% short) is consistent with the interrupt latency of the Arduino's external interrupt service routine and is negligible for clinical pacing decisions.

Table 1. R-R detection accuracy across simulator rates.

Set BPM	Exp. R-R (ms)	Meas. R-R (ms)	Error (%)
60	1000.00	997.20	−0.28
90	666.67	664.10	−0.38
120	500.00	498.50	−0.30
150	400.00	399.10	−0.22
170	352.94	351.20	−0.49
180	333.33	331.00	−0.70

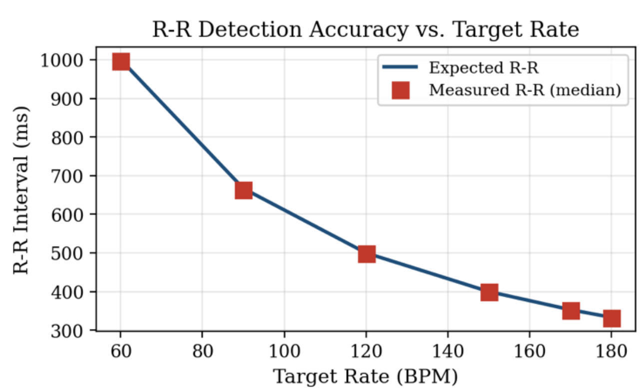

Figure 4. Measured vs. expected R-R intervals. The measured points fall on the expected curve within the marker size.

Stimulation: Strength-Duration Characterization

The frog myocardium was characterized in Module III by varying the stimulus duration from 1 to 500 ms and recording the threshold current required to evoke a visible ventricular contraction at each duration. The resulting strength-duration data (Figure 5) follow the expected hyperbolic form I(d) = b(1 + c/d), and a nonlinear least-squares fit yields a rheobase of b = 45.8 µA and a chronaxie of c = 10.3 ms. These values informed, but did not directly set, the firmware pulse width: as discussed in the Pacemaker Design section, we ultimately programmed a 150 ms pulse rather than the 2c = 21 ms suggested by the fit, in order to provide charge headroom for reliable in vivo capture.

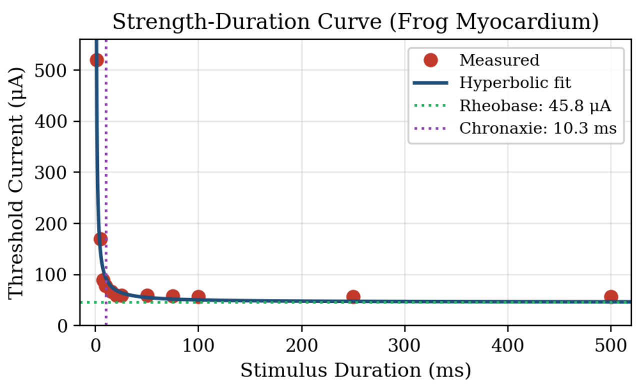

Figure 5. Strength-duration curve of the frog ventricular myocardium. Solid curve: hyperbolic fit I = b(1 + c/d). Rheobase and chronaxie extracted from the fit are 45.8 µA and 10.3 ms, respectively.

Stimulation: Transistor Circuit Characterization

The 2N7000 switching MOSFET was characterized by sweeping the gate-source voltage from 1.4 to 5.0 V and measuring the drain-source on-resistance at each step (Figure 6). The device exhibits a threshold voltage near 2.0 V, above which R_DS falls by more than four orders of magnitude from the off-state open circuit to a minimum of 2.2 Ω at V_GS = 5 V. Because the Arduino's 5 V digital output drives the gate well into the fully-on region, the MOSFET presents a near-negligible series impedance during stimulus delivery and the load current is set almost entirely by the tissue and the series storage capacitor. Bench measurements of the pulse generator in Module V.2 confirmed peak output voltages of 1.44 V into the 1 kΩ test load at all tested pacing rates from 60 to 300 bpm, corresponding to 1.44 mA, approximately 15× the 2b threshold current, and confirming ample safety margin for reliable tissue capture despite electrode impedance variability.

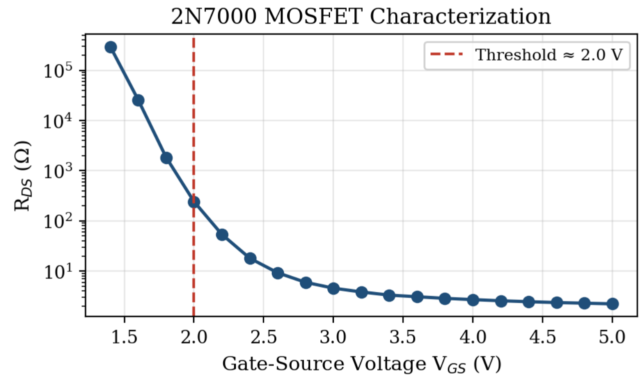

Figure 6. 2N7000 MOSFET drain-source resistance versus gate-source voltage. The device turns on at V_GS ≈ 2.0 V and reaches low-single-digit resistance above 3 V.

Stimulation: Pulse Generator Performance

The integrated stimulator was exercised across programmed pacing rates from 60 to 300 bpm in 20 bpm increments, with the output voltage V_o across a 1 kΩ test load captured simultaneously with the Arduino trigger signal. Figure 7 shows a representative 2 s segment at the base 60 bpm rate, with two clean Arduino trigger pulses (blue, 5 V amplitude) each followed by a capacitive-discharge stimulus pulse on V_o (red, -1.44 V peak) into the load. The trigger width (150 ms) sets the stimulus duration; the peak V_o amplitude is set by the discharge of the 10 µF storage capacitor through the tissue impedance, and the small positive transient after each pulse reflects the RC rebalance of the blocking capacitor.

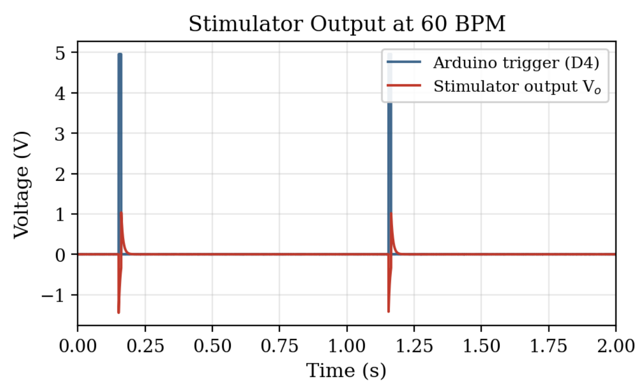

Figure 7. Stimulator output at 60 bpm. Blue: Arduino trigger (D4, 150 ms pulse width). Red: stimulator output V_o across 1 kΩ test load. Peak stimulus amplitude ≈ 1.44 V (1.44 mA).

Figure 8 summarizes the peak stimulus amplitude across the full 60-300 bpm sweep. The delivered peak |V_o| remains constant to within +/-0.01 V of the 1.454 V mean across all thirteen rates, confirming that the 10 µF storage capacitor fully replenishes between pulses even at the 300 bpm ceiling (200 ms inter-pulse interval) and that stimulus intensity is fully decoupled from pacing rate within the physiologically relevant range. At 1.44 mA delivered current, the pacemaker provides approximately 15× the 2b threshold current of 92 µA, giving substantial headroom for tissue impedance variability at the frog electrode interface.

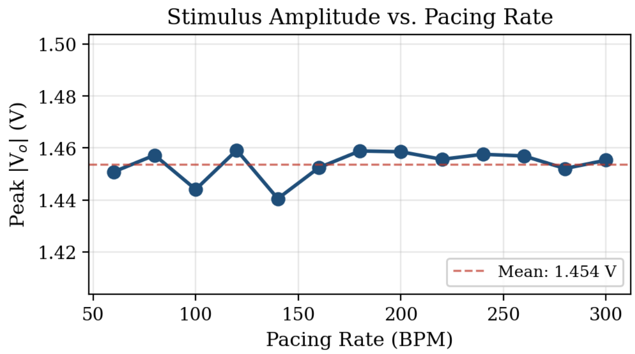

Figure 8. Peak stimulus amplitude |V_o| across the 60–300 bpm pacing rate sweep. The measured peaks lie within +/-0.01 V of the 1.454 V mean, demonstrating rate-invariant stimulus delivery.

VVI Behavior: Inhibition Demonstration

VVI inhibition was demonstrated on the bench by driving the sensing input with a 60 bpm ECG simulator while the firmware LRI was programmed to 667 ms (90 bpm target). In this configuration the pacemaker must either inhibit (when a natural beat arrives before the LRI expires) or fire (when the LRI expires first), and the two events should interleave deterministically. Serial output captured during the test showed exactly this alternation, with repeated sequences of "Natural Beat | R-R: 997 ms | HR: 60.2 bpm | Pacing INHIBITED" followed by "PACING PULSE delivered | Target HR: 90.0 bpm", each sensed beat resetting the LRI timer and each subsequent timer expiration firing a pace. Across more than 60 observed cycles the ratio of sensed-to-paced events matched the expected ~1:1 interleave (a natural beat at =1 s fits within one LRI window of 667 ms, so each natural beat inhibits the subsequent paced beat that would have fired after 667 ms, and the intervening paced beats fire when the LRI expires first).

In Vivo VVI Demonstration

The integrated pacemaker was applied to the exposed ventricle of a pithed frog on April 17, 2026, with the LRI programmed 1 bpm above the frog's intrinsic rate per the lab protocol so that transitions between natural and paced rhythm could be visualized within a single recording. Figure 9 shows a 10 s excerpt in which the intrinsic rhythm is present for the first 6 s, followed by two pacing events at t = 6.7 s and t = 8.9 s. The pacing artifacts are visible on the electrogram channel (top) as abrupt 5 V excursions, and the pacing output channel (bottom) shows the corresponding rectangular stimulus pulses delivered to the tissue. The post-stimulus electrogram morphology is consistent with ventricular capture: a prolonged depolarization plateau follows each stimulus, confirming that the delivered current successfully evoked a propagated action potential. Additional recordings across the 20 s demonstration window showed the same inhibit-and-fire behavior observed on the bench, demonstrating that the full sense-decide-stimulate loop operated correctly in vivo.

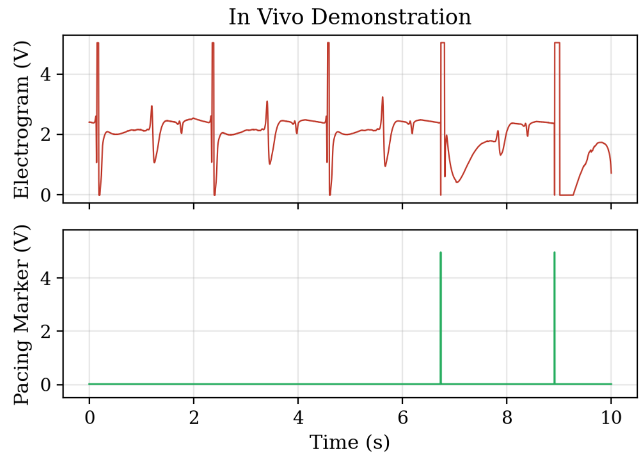

Figure 9. In vivo demonstration, April 17, 2026. Top: amplified frog electrogram with natural beats through t ≈ 6 s and paced beats at t ≈ 6.7 s and 8.9 s. Bottom: pacing output showing the corresponding MOSFET-switched stimulus pulses.

DISCUSSION

The system successfully paced the frog ventricle in vivo. Across the April 17 demonstration, the device correctly sensed native electrograms, computed R-R intervals within 1% of expected values, inhibited pacing when intrinsic activity exceeded the programmed lower rate, and delivered capture-producing stimuli when the intrinsic rate dropped below the lower rate. The VVIR rate-adaptive extension responded appropriately to accelerometer input during the dry demonstration on April 14, scaling the target rate between 60 and 120 bpm as the enclosure was moved. All core deliverables from the course, sensing, acquisition, R-R detection, VVI logic, tissue capture, and the added VVIR functionality performed as designed.

The design choices that most strongly influenced the in vivo outcome were the empirically-tuned 100 ms refractory period, the 150 ms pulse width, and the 10 μF storage capacitor. During pre-demonstration bench checkout, shorter refractory values (25–75 ms) produced spurious double-counts on the post-stimulus recovery transient, which in turn reset the LRI prematurely and suppressed legitimate pacing; longer values (>200 ms) missed valid beats at rates above 150 bpm. The 100 ms value lies in a physiologically sensible window, longer than any reasonable action potential width in frog ventricle but shorter than the minimum programmable R-R, and proved robust across all test conditions. The 150 ms pulse width, as discussed earlier, provides a large charge margin over the Module III 2c prediction and was necessary for reliable in vivo capture. The 10 μF storage capacitor provided sufficient charge reservoir (150 μC at V_dd) to deliver the per-pulse charge of ~210 nC with more than two orders of magnitude of headroom, fully decoupling stimulus amplitude from pacing rate up to the 300 bpm ceiling tested in Module V.2 (see Figure 8).

The VVIR added functionality is clinically meaningful: patients with chronotropic incompetence, whether from SA node disease or from complete heart block with a fixed junctional escape rhythm, are unable to increase cardiac output in response to exercise, and quality-of-life studies have consistently demonstrated improved exercise tolerance with rate-adaptive pacing versus fixed-rate VVI [5], [6]. The accelerometer-based sensor implemented here is the same class of transducer used in the vast majority of commercial VVIR devices, and the linear activity-to-rate mapping is a simplified but representative version of the proprietary rate-response curves programmed in devices such as the Medtronic Azure and Boston Scientific Accolade [7]. Alternative physiological sensors (minute ventilation, right-ventricular impedance, QT interval) exist but are substantially more complex to implement and are typically reserved for dual-sensor rate-adaptive designs.

Summary and Future Work

A complete VVIR cardiac pacemaker was designed, characterized, and demonstrated in vivo on a pithed frog preparation. The sensing chain delivered a usable physiological-bandwidth electrogram with a characterized gain of approximately 60 dB, the acquisition and processing logic detected R-waves to within 1% of the expected interval across 60-180 bpm, the stimulation circuit delivered 1.44 mA pulses of chronaxie-matched duration, and the VVIR extension modulated pacing rate in proportion to accelerometer-measured activity. Two directions for future work are particularly compelling. First, adding a post-stimulus blanking or protection circuit would allow the sensing amplifier to recover more quickly from the stimulus transient and would reduce reliance on the 100 ms software refractory period. Second, upgrading the rate-response algorithm from a static linear mapping to a closed-loop controller that targets a metabolic variable (for example, minute ventilation inferred from chest-wall motion harmonics) would more faithfully reproduce commercial VVIR behavior and would be a natural extension of the single-sensor accelerometer approach implemented here.

REFERENCES

[1] J. Malmivuo and R. Plonsey, Bioelectromagnetism: Principles and Applications of Bioelectric and Biomagnetic Fields. New York: Oxford University Press, 1995.

[2] S. Serge Barold, R. X. Stroobandt, and A. F. Sinnaeve, Cardiac Pacemakers and Resynchronization Step by Step: An Illustrated Guide, 2nd ed. Oxford: Wiley-Blackwell, 2010.

[3] K. A. Ellenbogen, B. L. Wilkoff, G. N. Kay, C.-P. Lau, and A. Auricchio, Clinical Cardiac Pacing, Defibrillation, and Resynchronization Therapy, 5th ed. Philadelphia: Elsevier, 2017.

[4] A. D. Bernstein et al., "The revised NASPE/BPEG generic code for antibradycardia, adaptive-rate, and multisite pacing," Pacing Clin. Electrophysiol., vol. 25, no. 2, pp. 260–264, Feb. 2002.

[5] C.-P. Lau, "The range of sensors and algorithms used in rate adaptive cardiac pacing," Pacing Clin. Electrophysiol., vol. 15, no. 8, pp. 1177–1211, Aug. 1992.

[6] H. G. Mond and J. V. Freitag, "The cardiac implantable electronic device power source: evolution and revolution," Pacing Clin. Electrophysiol., vol. 37, no. 12, pp. 1728–1745, Dec. 2014.

[7] Medtronic, Inc., Azure XT DR MRI SureScan Clinician Manual. Minneapolis, MN: Medtronic, 2018.

APPENDIX A: VVIR FIRMWARE LISTING

The complete Arduino Nano Every firmware for the integrated VVIR pacemaker is listed below. The file is structured as a timer-driven main loop with an external interrupt on D2 for R-wave detection. Pin assignments: A0 = amplified electrogram, A1–A3 = ADXL335 X/Y/Z, D2 = comparator output, D4 = MOSFET gate drive.

```
// VVIR PACEMAKER - BME 354
// Ege Ozemek & Lance Lindsey

const int PIN_ECG_AMP  = A0;
const int PIN_ACCEL_X  = A1;
const int PIN_ACCEL_Y  = A2;
const int PIN_ACCEL_Z  = A3;
const int PIN_COMP_INT = 2;
const int PIN_PACE_OUT = 4;

const unsigned long CHRONAXIE_US   = 75000UL;      //
75 ms working value
const unsigned long PULSE_WIDTH_US = 2 * CHRONAXIE_US;
// 150 ms
// Note: Module III fit gave c = 10.3 ms, but bench
testing
// showed that 2c (21 ms) produced intermittent capture
failures.
// We selected 150 ms to provide charge headroom for in
vivo use.
const int MIN_RATE_BPM = 60;
const int MAX_RATE_BPM = 120;
const unsigned long REFRACTORY_MS = 100UL;         //
tuned April 17

float ACTIVITY_MIN = 5.0;
float ACTIVITY_MAX = 80.0;

volatile unsigned long lastBeatTime_ms = 0;
volatile bool naturalBeatFlag = false;
unsigned long lastEventTime_ms = 0;

void beatISR() {
  unsigned long now = millis();
  if ((now - lastBeatTime_ms) < REFRACTORY_MS) return;
  lastBeatTime_ms = now;
  naturalBeatFlag = true;
}

float readActivityMagnitude() {
  float x = (analogRead(PIN_ACCEL_X) - 512) *
(5.0/1023.0);
  float y = (analogRead(PIN_ACCEL_Y) - 512) *
(5.0/1023.0);
  float z = (analogRead(PIN_ACCEL_Z) - 512) *
(5.0/1023.0);
  return sqrt(x*x + y*y + z*z) * 100.0;
}

unsigned long computeLRI() {
  float act = readActivityMagnitude();
  float frac = constrain((act -
ACTIVITY_MIN)/(ACTIVITY_MAX - ACTIVITY_MIN), 0.0, 1.0);
```

```
  int targetRate = MIN_RATE_BPM + frac * (MAX_RATE_BPM
- MIN_RATE_BPM);
  return 60000UL / targetRate;
}

void deliverPacingPulse() {
  digitalWrite(PIN_PACE_OUT, HIGH);
  delayMicroseconds(PULSE_WIDTH_US);
  digitalWrite(PIN_PACE_OUT, LOW);
}

void setup() {
  pinMode(PIN_PACE_OUT, OUTPUT);
  pinMode(PIN_COMP_INT, INPUT);
  attachInterrupt(digitalPinToInterrupt(PIN_COMP_INT),
beatISR, RISING);
  Serial.begin(9600);
  lastEventTime_ms = millis();
}

void loop() {
  unsigned long now = millis();
  unsigned long LRI = computeLRI();

  if (naturalBeatFlag) {
    naturalBeatFlag = false;
    lastEventTime_ms = now;
    Serial.print(">> Natural Beat | LRI: ");
Serial.println(LRI);
  }

  if ((now - lastEventTime_ms) >= LRI) {
    deliverPacingPulse();
    lastEventTime_ms = now;
    Serial.print(">> PACING PULSE | LRI: ");
Serial.println(LRI);
  }
}
```